

SCIENTIFIC REPORTS



OPEN

Gene-set Analysis with CGI Information for Differential DNA Methylation Profiling

Chia-Wei Chang^{1,*}, Tzu-Pin Lu^{1,2,*}, Chang-Xian She¹, Yen-Chen Feng^{1,3} & Chuhsing Kate Hsiao^{1,2}

Received: 15 October 2015

Accepted: 30 March 2016

Published: 19 April 2016

DNA methylation is a well-established epigenetic biomarker for many diseases. Studying the relationships among a group of genes and their methylations may help to unravel the etiology of diseases. Since CpG-islands (CGIs) play a crucial role in the regulation of transcription during methylation, including them in the analysis may provide further information in understanding the pathogenesis of cancers. Such CGI information, however, has usually been overlooked in existing gene-set analyses. Here we aimed to include both pathway information and CGI status to rank competing gene-sets and identify among them the genes most likely contributing to DNA methylation changes. To accomplish this, we devised a Bayesian model for matched case-control studies with parameters for CGI status and pathway associations, while incorporating intra-gene-set information. Three cancer studies with candidate pathways were analyzed to illustrate this approach. The strength of association for each candidate pathway and the influence of each gene were evaluated. Results show that, based on probabilities, the importance of pathways and genes can be determined. The findings confirm that some of these genes are cancer-related and may hold the potential to be targeted in drug development.

DNA methylation (DNAm) occurs when a methyl group is added to the cytosine in CpG dinucleotides. The presence of such methyl groups can modify DNA and thus alter gene expression. Because DNAm is more stable than gene expression and can represent long-term environmental influences, it may serve as a good candidate biomarker for disease diagnosis, disease prognosis or therapy response prediction^{1,2}. Acting as an intermediary between genome sequences, environmental influences and gene expression, DNA methylation is a common epigenetic tool that plays an important role in several processes, including those of development and genomic imprinting, and therefore is linked to risk of various diseases^{1,3,4}.

DNAm patterns depend on whether CpGs locate in CpG islands (CGIs)^{5–8}. CpG islands—defined as upstream CG-rich regions with length greater than 200 bps, GC content greater than 50%, and an observed-to-expected CpG ratio greater than 0.6—are often associated with transcription start sites (TSS)⁹. CGIs may cause gene silencing and transcriptional aberrations, as shown in various types of cancers^{7,8,10–12}. In normal cells, methylation mainly occurs at repetitive elements or intergenic regions, while CpG island promoters of genes are usually less methylated or not methylated at all. In cancer cells, however, methylation at non-coding regions is transferred by DNA methyltransferase to CpG island promoters, causing the CGIs to become hypermethylated. These hypermethylated CGIs are thought to block the transcription of tumor suppressor genes, leading to abnormal cell growth^{6,11,12}.

Another issue of concern in the analysis of DNA methylation, as in any analysis of genetic studies, is the need to incorporate biological information for more intuitive and appropriate interpretations. For instance, since most genes do not work alone, inclusion of known information about relationships among a set of genes can help scientists to better evaluate the effect on disease development of the set of genes working jointly. In their consideration of pathways as gene-sets, most current analyses treat the genes located in the same pathway as independent entities. Examples include the knowledge-based pathway analyses, such as over-representation analysis (ORA) and functional class scoring (FCS), which investigate whether certain genes of interest are differentially expressed

¹Institute of Epidemiology and Preventive Medicine, College of Public Health, National Taiwan University, Taipei 10055, Taiwan. ²Bioinformatics and Biostatistics Core, Center of Genomic Medicine, National Taiwan University, Taipei 10055, Taiwan. ³Department of Epidemiology, Harvard School of Public Health, Harvard University, Boston, MA 02115, U.S.A. *These authors contributed equally to this work. Correspondence and requests for materials should be addressed to C.K.H. (email: ckhsiao@ntu.edu.tw)

in given pathways. These approaches consider the pathway simply as a set of independent units, ignoring possible interaction and regulation between components in the same pathway. To account for the position of a gene in a pathway, sometimes called the *pathway topology*, the Impact Factor was later proposed to measure changes in a given pathway when perturbation occurs¹³. This analysis was further modified to rank pathways¹⁴. The resulting tool allows the same gene to have multiple functions in different pathways, but does not assume the existence of possible interwoven relationships (cross-talk) between pathways. Identification of susceptible genes that includes simultaneous consideration of both their pathway information and the distinctive roles they play in different pathways¹⁵, remains a challenging task.

Another concern arising in the analysis of DNA methylation is confounders. Factors underlying observed variability in DNA methylation include tissue type, cell type, age, and gender^{16–20}. Specifically, several studies have identified CpG sites whose methylation levels were associated with age under a cross-sectional or longitudinal study design^{16,21–23}, using Infinium HumanMethylation27 BeadChip (Illumina Inc., San Diego, CA, USA) or Infinium HumanMethylation450 BeadChip (Illumina Inc.). Recently, Florath *et al.*²¹ considered a population-based cohort study to identify, and then later to confirm with an independent cohort, more than one hundred CpG sites with methylation levels significantly associated with age. Therefore, it is not surprising that much emphasis has been placed on the importance of designing studies that use twins or age-matched case-controls to adjust for confounders, before making inferences on the association between CpG methylation and diseases^{20,23}.

To simultaneously include both CGI status and pathway information in the association analysis, as well as to account for heterogeneity across subjects and possible confounders, we propose functions to model the CGI information and pathway knowledge, under an age-matched case-control study design. We adopt the Bayesian approach for its flexibility in modeling stochastic epigenetic variation, such as random individual effects^{5,24} and a probe-specific CGI effect that depends on whether or not the probe locates in a CGI. For the pathway association, our model allows that all genes in the same pathway share a common base effect, but that the overall effect of an individual gene can increase or decrease according to its position in the gene-set, which may be related to, for example, the number of neighboring genes it connects to. Previous Bayesian inference on DNA methylation studies assumed that every CpG locus was exchangeable and thus assigned it an equal effect^{25,26}. Our proposed model aims to relax this assumption for more general cases. To illustrate the methodology, we consider three cancer studies with 104, 32, and 16 case-control pairs, respectively. The first two applications are of DNA bisulfite methylation profiling from ovarian and lung cancer studies^{20,27} and the third is of NGS methylation profiling, by reduced representation bisulfite sequencing (RRBS) of high-grade ductal carcinoma *in situ* (HG-DCIS), from a breast cancer study²⁸.

Results

An overview of the procedures, including subject matching, examination of CGI status, and construction of gene-set information, is outlined in Fig. 1. To illustrate how the above model and functions can be applied, we consider first the United Kingdom Ovarian Cancer Population Study (UKOPS)²⁰. The DNA methylation data are available from the GEO database (accession number GSE19711) with 27,578 CpGs per sample. The methylation level of each specific CpG site was calculated from the intensity values of methylated and unmethylated DNA beads as a ratio of fluorescent signals, called β values. The procedures for data management—outlier detection and removal of batch effect, normalization, and matching—are explained in Supplementary Text S1, available online. To remove the confounding effect due to age, we matched the case-control pairs by restricting the difference in age to be less than three, obtaining 104 case-control pairs for subsequent analysis.

The second application involves methylation profiling from tumor and adjacent normal tissues of 32 patients with lung adenocarcinoma²⁷. This study provides a perfect matching design for reducing possible confounding effects. The data can be accessed from NCBI GEO database with accession numbers GSE19804 and GSE49996. For the third application, we consider next-generation sequencing DNA methylation by RRBS from a study of pure high-grade ductal carcinoma *in situ* of 23 breast cancer patients and 5 normal controls²⁸. This type of data is uncommon and often of small sample size. Therefore, we match every normal control with more than 1 cancer patient of the same ethnic group and similar age (less than 5 years). This third data set contains 16 pairs. The original data can be downloaded from NCBI GEO database with accession number GSE69994.

Stratification by CpG island status. To examine by figures whether DNA methylation varies according to CpG island status, boxplots of the pair-wise differences in DNAm θ_{ij} from 100 randomly selected probes were constructed (Fig. 2A) for the UKOPS study. This figure included 76 probes located in CGIs (called CGI probes) and 24 located outside (called non-CGI probes). It can be readily observed that the differences in DNAm show larger variability when the probes are located in CGIs (colored in red); while the probes located outside of CGIs (colored in black) tend to have smaller dispersion. In fact, among the original 27,578 probes, the means of the θ_{ij} were -1.1×10^{-3} and -5.8×10^{-4} , respectively ($p < 1 \times 10^{-7}$), supporting the assumption that CGI probes and non-CGI probes are not homogeneous. Moreover, probes of the same CGI status tend to have similar values of θ_{ij} . Figure 2B shows the correlation between non-CGI probes and the correlation between CGI probes. A clear pattern emerges; probes are more alike if they are of the same CGI status. Both Fig. 2A,B support the assumption that the effect of CGI status β_j for probe j can be assumed to come from one of two distributions, depending on the CpG island status of the probe. Similarly, the pattern of heterogeneous variation is apparent in the differences in DNAm among the 32 pairs of the lung cancer data. The boxplots of θ_{ij} from 200 randomly selected probes in CGIs and from 200 not in CGIs show different degrees of variability, as seen in Supplementary Fig. S1a,b. For the NGS methylation data, the number of pairs is only 16, and thus no boxplot is produced.

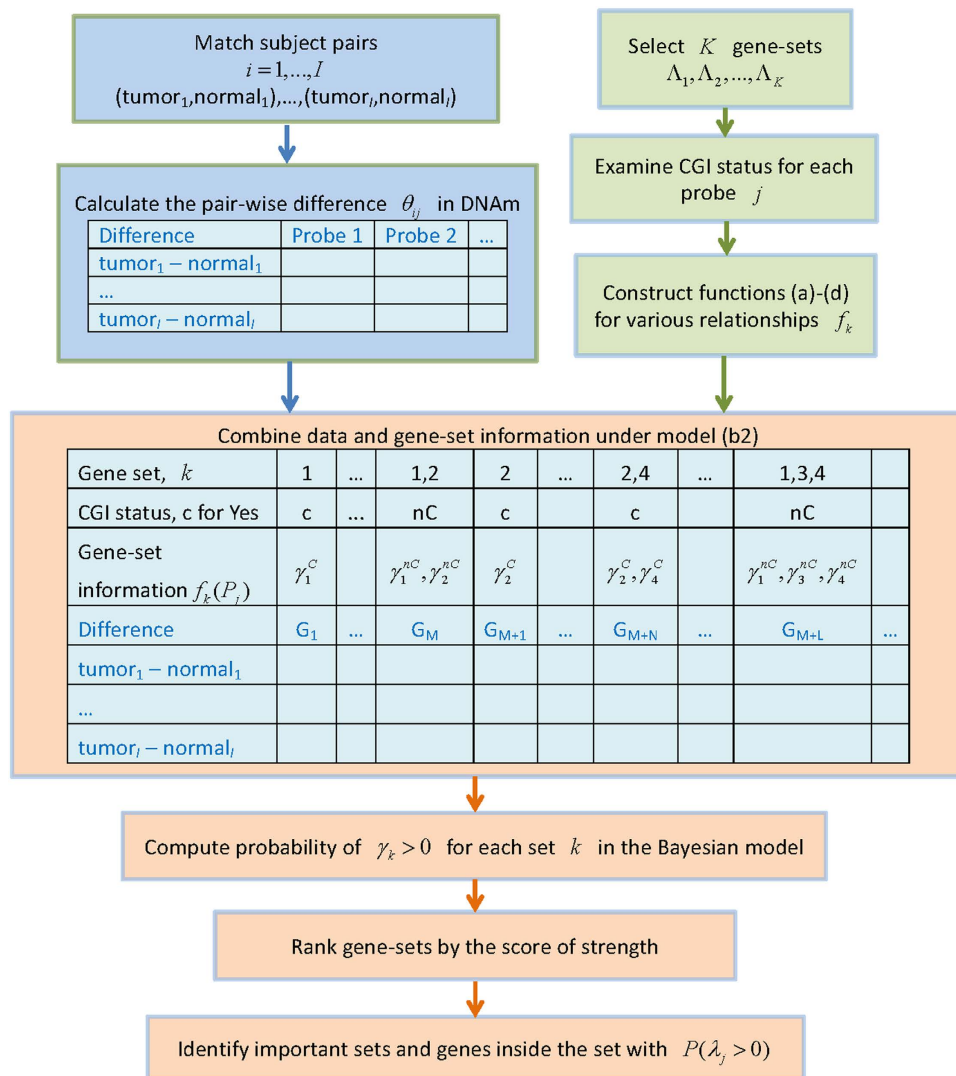


Figure 1. Overview of procedures.

Incorporation of biological pathway information. For the UKOPS study, we selected ten competing pathways defined in KEGG (Kyoto Encyclopedia of Genes and Genomes). The ten sets involve 1,675 probes in 795 genes and the ten pathways have been reported to associate with ovarian cancer²⁹. Among the ten pathways, four (drug metabolism - cytochrome p450, metabolism of xenobiotics by cytochrome p450, tyrosine metabolism, and arginine and proline metabolism) are associated with the metabolism of xenobiotics or amino acids; while another 4 pathways (focal adhesion, cell cycle, p53 signaling pathway, and oocyte meiosis) are related to cellular processes such as cell communication or cell growth and death. These ten pathways are not of equal size. The tyrosine metabolism pathway is relatively small with 31 genes covered by 57 methylation probes; while the “pathways in cancer” pathway is huge with 303 genes covered by 714 probes. The numbers involved in the other pathways are listed in the first column in Table 1. For the lung cancer DNAm, the number of pairs is only 32 and thus only four signaling pathways were selected: axonal guidance, GNRH, prolactin, and glycosphingolipid biosynthesis. These four pathways contain 103, 58, 46, and 24 genes, respectively. For the 16 pairs matched from the NGS methylation data, we consider only two signaling pathways (mTor and p53) to avoid instability in estimation due to the small sample size. These two pathways contain a total of 2,468 probes in 71 genes.

To illustrate how to evaluate the pathway effects, we denote first the CGI-dependent effect β_j for each probe P_j , where $j = 1, \dots, 1,675$ for the UKOPS data. Each probe P_j was examined first to see if its corresponding gene G_j falls in the k th pathway where $k = 1, \dots, 10$. Note that the same gene can occur in more than one pathway, i.e. the indicator function $I_k(P_j)$ can be 1 for more than one k . Figure 3 provides a hypothetical gene-set. In each gene node, its CGI status is 1 ($I_k(P_j) = 1$) if P_j is in a CGI, E_{jk} is the number of neighbors of gene G_j in the k th pathway. No differentiation is made between the incoming and outgoing edges in the current settings. For selecting the best model, we adopt deviance information criterion (DIC), a common measure for Bayesian model selection. Other details of the specifications, computations, and the codes to be used in the R package R2OpenBUGS are listed in Supplementary Text S1.

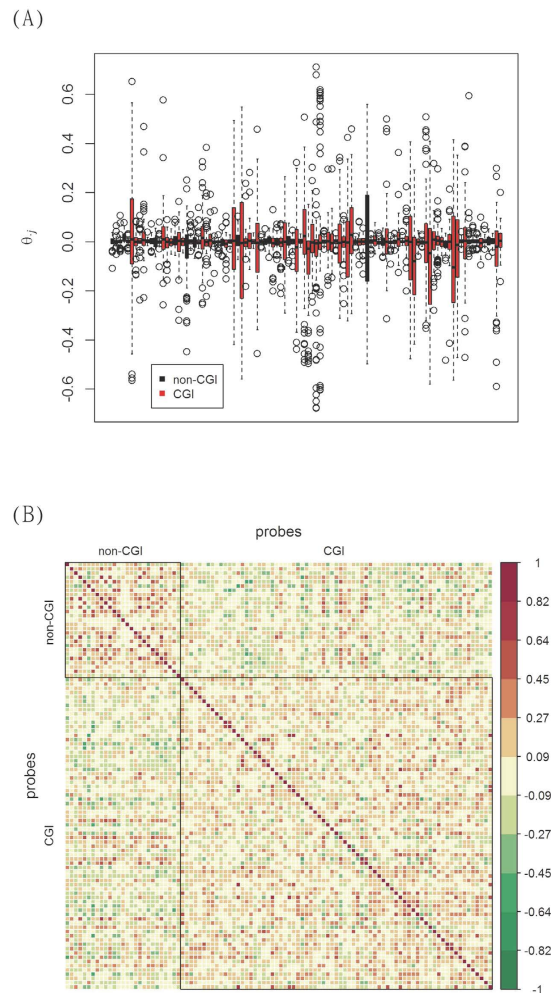


Figure 2. DNAm and CGI status. (A) Boxplots of differences in DNAm between matched pairs of ovarian cancer patients (cases) and normal controls for 100 randomly selected probes. The 76 red boxplots are for probes in CGI region; while the 24 black boxplots are for probes not in CGI. Probes in CGI tend to have larger variation in θ_{ij} , indicating a larger degree of variability in DNAm between cases and controls. (B) Correlation plots of θ_{ij} . The upper left panel contains correlations of θ_{ij} from probes not in CGI; while the lower right panel is for probes in CGI. The correlation in each panel is larger, as compared to the correlations in the other two blocks, indicating a greater degree of similarity in θ_{ij} , the differences in DNAm.

Evaluation of pathway effects. To infer the pathway effect γ_k , we derived the estimated posterior probability of positive γ_k for each pathway, conditioning on the observed methylation levels $\theta = \theta_{ij}$. If the probability $P(\gamma_k > 0 | \theta = (\theta_{ij}))$ is close to 1, it implies that, on average, genes in this pathway were more hypermethylated in cancer patients. On the other hand, a probability close to zero indicates that γ_k was mostly negative, implying hypomethylation for the genes in the k th pathway.

UK Ovarian Cancer Population Study. Table 1 lists the probability of hypermethylation $\Pr(\gamma_k > 0)$ among cancer patients for each pathway under different models. The top two pathways, the pathways in cancer and the cell cycle pathway, correspond to the two most extreme probabilities. For the pathways in cancer, the probability was close to zero (e.g., 0.01 under model (b1)), indicating a general pattern of hypomethylation in this pathway. In other words, cancer patients were the least hypermethylated in this group. This pathway consists of several signaling networks (such as the p53 signaling pathway and the cell cycle pathway) related to cancer prognosis, including those of tissue invasion and metastasis, sustained angiogenesis, evading apoptosis, proliferation, failed repair of genes, insensitivity to anti-growth signals, genomic damage, resistance to chemotherapy, and blocking of differentiation. Several genes within this pathway have been reported to show association with ovarian cancer, including Cyclin D1 (*CCND1*), *CDK2*, *ERB2*, and *EGFR*. The cyclins function as regulators of Cyclin-dependent kinases (CDKs) and play an important role in the cell cycle G1/S transition. The four aforementioned genes in this pathway have all been suggested as biomarkers for various cancers.

The probability of the cell cycle pathway was close to 1 (Table 1), implying strong support of hypermethylation for this pathway. Similarly for model (b2), the probability of hypermethylation for probes in CGIs was as high as 0.97. In other words, ovarian cancer subjects hypermethylated to a greater degree than healthy subjects in this

KEGG pathway term (no. of genes/no. of probes)	Constant effect model			Degree effect model		
	(b1) CGI-independent	(b2) CGI-dependent		(c1) CGI-independent	(c2) CGI-dependent	
		Y	N		Y	N
hsa05200 Pathways in cancer (303/714)	0.01	0.02	0.03	0.19	0.10	0.35
hsa04110 Cell cycle (120/308)	0.96	0.97	0.44	0.84	0.89	0.55
hsa04114 Oocyte meiosis (101/211)	0.21	0.14	0.65	0.23	0.18	0.56
hsa00980 Metabolism of xenobiotics by cytochrome P450 (69/122)	0.30	0.31	0.50	0.56	0.17	0.74
hsa00330 Arginine and proline metabolism (53/100)	0.44	0.25	0.70	0.51	0.27	0.68
hsa04510 Focal adhesion (192/418)	0.50	0.45	0.69	0.49	0.45	0.59
hsa04610 Complement and coagulation cascades (64/113)	0.43	0.25	0.41	0.59	0.24	0.54
hsa00982 Drug metabolism - cytochrome P450 (63/111)	0.62	0.46	0.47	0.41	0.66	0.28
hsa00350 Tyrosine metabolism (31/57)	0.49	0.43	0.43	0.48	0.24	0.45
hsa04115 p53 signaling pathway (67/201)	0.32	0.50	0.38	0.57	0.68	0.20

Table 1. Numbers are the posterior probability of $\gamma_k > 0$ under the specified model for the UKOPS study. Values closer to 1 imply stronger evidence of hypermethylation in cases than in controls; while values closer to 0 indicate stronger evidence of hypomethylation.

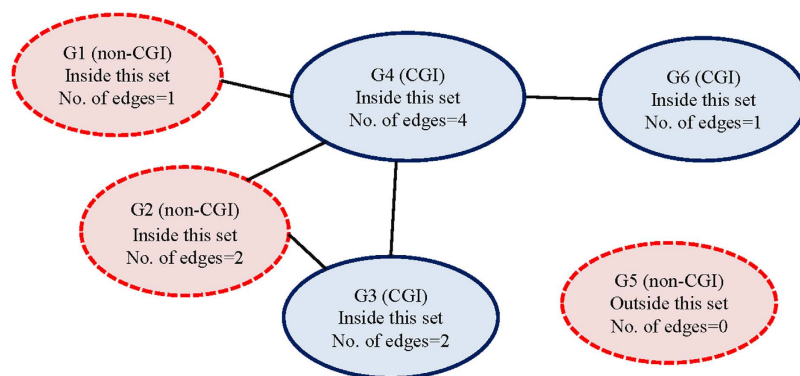


Figure 3. A hypothetical gene-set. Gene nodes in red (G1, G2, and G5) contain no probes in CGIs; while nodes in blue (G3, G4, and G6) contain probes in CGI regions. All gene nodes but G5 belong to this gene-set. The number of edges represents the number of genes connected to it.

pathway. Indeed this pathway regulates all steps in the mitotic cell cycle, including DNA replication (S phase), mitosis (M phase) and the gaps (G1 and G2 phases)^{30,31}. The pathway includes genes such as *ATM*, *CCND1*, *CDK2*, *CCNB2*, and *CHEK2* that are known to be involved in carcinogenesis.

An alternative way to compare these pathways is to rank the distances between the probabilities in Table 1 and 0.5 (i.e., no difference). For the purpose of easy interpretation, we rescaled the distance by multiplying by 2, making the distance range from 0 to 1, and called it the score of strength. Figure 4A plots the scores for the corresponding pathways. Clearly the top two pathways stand out. Details of the values are in Supplementary Table S1. To assess which model was most promising for further inference, we considered the DIC (Deviance Information Criterion) under each model. No specific model fitted better than the others, hence the model with the CGI-dependent pathway effect (model (b2)) was selected based on the principle of parsimony and for its better interpretability. The resulting model (b2) was then used to detect influential genes and was compared with other analyses, as discussed in the next section.

Lung Adenocarcinoma Study. To evaluate the strength of pathway effect by assigning it a probability, Fig. 4B,C are boxplots and density plots of the four pathway effects, where the axonal guidance signaling pathway ranks as the most important pathway. In this pathway, tumor tissues generally contained hypermethylated CpG sites (with a probability of 0.97); while in the glycosphingolipid biosynthesis signaling pathway, tumor tissues tended to be

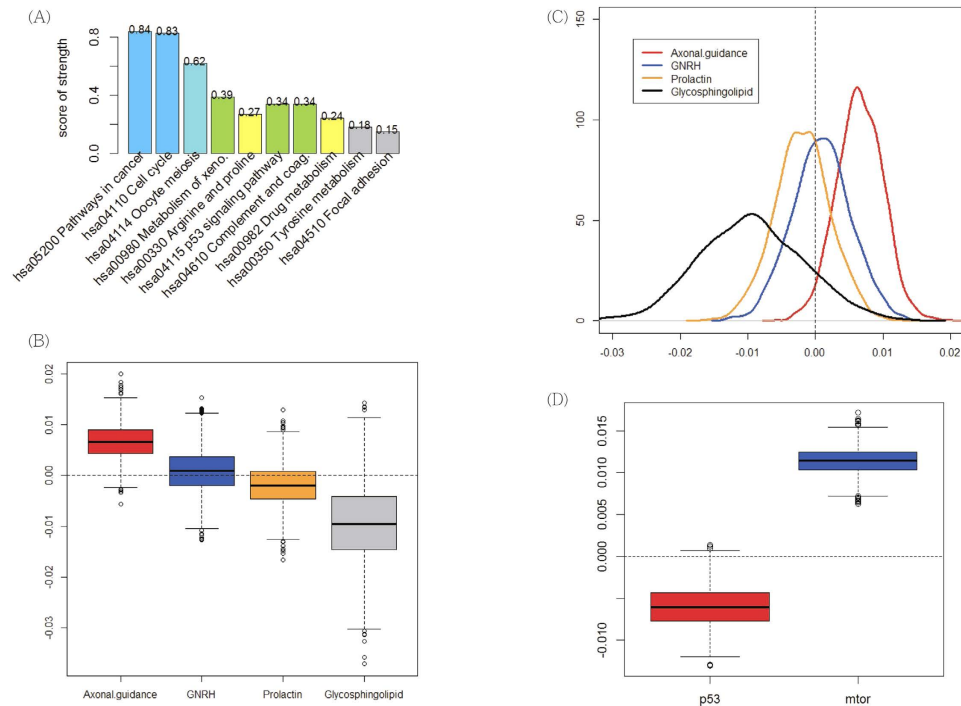


Figure 4. (A) Plots of pathway effects. (A) Scores of strength for the 10 competing pathways in the UKOPS study. (B) Boxplots of posterior samples under each pathway for 32 lung adenocarcinoma patients. A box beyond zero implies a large probability of hypermethylation; while a box below zero indicates a large probability of hypomethylation. (C) Probability density plot for each of the four pathway effects. Most of the red curve for the effect of axonal guidance signaling pathway locates in the positive part, indicating a strong hypermethylation effect for this pathway. (D) Boxplots of posterior samples in each pathway in the breast cancer study.

hypomethylated (with a probability of 0.88). As for the GNRH pathway, the probability that tumor tissues were hypermethylated was estimated to be 0.58, and for glycosphingolipid biosynthesis the probability of hypomethylation was 0.69.

HG-DCIS Breast Cancer Study. The boxplots in Fig. 4D illustrate the two pathway effects. The effect of p53 pathway is mostly negative, indicating a strong hypomethylation pattern in cases (probability 0.99). In contrast, the mTor pathway shows a moderate hypermethylation pattern among the HG-DCIS patients (probability larger than 0.99). The results not only confirm the importance of these two pathways, but also quantify the effect and its direction of these pathways.

Disease-related genes. Within the top-ranked pathways, we next examined the differentially methylated probes and genes for disease association with the probe-specific effect λ_j . This quantity summarizes the influence from both CGI status and the pathway. If λ_j locates far away enough from zero that either one of the posterior probabilities $\Pr(\lambda_j > 0)$ or $\Pr(\lambda_j < 0)$ is large, say greater than 0.975, then this probe is considered a methylation variable probe. Consequently, its corresponding gene is defined as a differentially methylated gene (DMG). In Bayesian statistical inference, the magnitude of the probability (Bayesian posterior probability, BPP^{32–34}) stands for the strength of evidence. Thus, depending on the context, one can select any large value (usually larger than 0.80) as the threshold. Here we used 0.975 simply to focus on the first few leading GO terms.

UK Ovarian Cancer Population Study. Under model (b2), 61 DMGs in the pathways in cancer and 14 DMGs in the cell cycle pathway were identified. Among the 61 DMGs identified in the pathways in cancer under model (b2), only 7 have passed the single-marker paired t-test with Bonferroni correction ($p < 3 \times 10^{-5}$); while none among the 14 DMGs in the cell cycle pathway passed the test. Next, we searched PubMed with the query string “human methylation ovarian cancer” and with “human ovarian cancer” and tallied, for each gene that appeared in more than one study, the total number of studies in which a given gene had been reported to be associated with ovarian cancer as of 10 April 2014. Among the 61 DMGs, 32 had been previously reported to associate with ovarian cancer; while 9 among the 14 DMGs in the cell cycle pathway had been previously reported. Examples are *CDKN2A* and *PTEN*, known tumor suppressors in multiple cancers; *EGFR* and *KDR*, known cancer genes; and *RUNX1* and *STAT3*, recently discovered to affect epithelial cancers^{35–38}. Most of the DMGs were detected with probes showing more hypermethylation in controls than in cases (probability larger than 0.975). Exceptions include *CCND1*, *BCL2*, *ERBB2*, and *RARB* genes containing hyper- and hypo-methylation probes, and *FRAP1*,

Gene symbol	
Previously reported (35 genes)	
In both pathways	CCND1 ^a , CDKN2A, CDKN2B, CDK2, CDKN1A, SMAD2
In pathways in cancer	APPL1, BAX, BCL2 ^a , DCC, EGFR, ERBB2 ^a , EGF23, EGF3, EGF4, EGF5, EGF8, FOXO1, FRAP1 ^b , IL6, KITLG, LAMB2, MMP2, MMP9, PTEN, PTK2, RARB ^b , RUNX1 ^b , STAT3 ^b , STAT5A, TGFBR1, WNT2
In cell cycle pathway	ATM ^b , CCNB2 ^b , CHEK2 ^b
Previously unknown (33 genes)	
In both pathways	CCNA1
In pathways in cancer	ARNT2, BIRC2, CSF3R, CUL2, CYCS, FASLG, FGF10, FGF12, FGF17, FGF19, FZD10, FZD8, HSP90AB1, JUP, LAMA1, LAMA4, NKX3-1, PIK3CD, PRKCB, PITCH2, RALGDS, RASSF5, RXRB, SMO, SPI1, WNT10A, WNT11, WNT3A
In cell cycle pathway	ESPL1, MCMA4, TFDPI, YWHAQ
Previously reported DMGs in other pathways (11 genes)	
	COL1A1, COL6A1 ^b , CRI, GSTP1, IGFBP3, KDR, MOS, PGR, PLAU, PPP2R1B, TP73

Table 2. Gene symbols of the 61 DMGs identified in the pathways in cancer, and 14 DMGs identified in the cell cycle pathway. ^aThese genes contain both hyper- and hypo-methylated probes. ^bThese genes contain probes that are more hypermethylated in cases than in controls.

RUNX1, *STAT3*, *ATM*, *CCNB2*, *CHEK2*, and *COL6A1* genes containing probes that are more hypermethylated in cases than in controls. Table 2 lists the names of these genes. Some of these genes have been considered as candidates for targeted cancer therapeutics. Our results suggest that DNA methylation can play a role in the development of such drugs. Supplementary Figure S2 demonstrates the location of these genes in the pathway map.

Lung Adenocarcinoma Study. Figure 5A is the heatmap of θ_{ij} for the leading genes in each of the four competing pathways. Most genes in the axonal guidance signaling pathway showed a hypermethylation effect in tumor tissue; while most in the prolactin signaling pathway and glycosphingolipid pathway showed hypomethylation. Within each pathway, the DMGs with large probability of hypermethylation and hypomethylation are listed in Table 3 and Supplementary Table S2. Although the major function of the axonal guidance signaling pathway is to regulate the growth of neuronal cells, many studies have reported its association with lung cancer^{39–41}. For instance, migration and invasion in lung adenocarcinoma cells can be substantially inhibited through the blockage of the complex *LIMK1/PAK4/cofilin*⁴², and methylation changes of *CDKN2A* may interact with *HRAS* to regulate the activity of *MAPK1* in lung adenocarcinoma⁴³. Table 3 also lists the expression changes of genes in this pathway. Regarding the other three pathways shown in Table S2, previous reports have indicated their biological impact in lung cancer with expression data as well^{44–47}. Therefore, these results further demonstrate that methylation change is a causative mechanism in regulating the activity of signaling pathways involved in tumor development and growth.

HG-DCIS Breast Cancer Study. Table 4 lists gene symbols of probes with large probabilities of hypermethylation and hypomethylation among patients with HG-DCIS. Note that the mTor pathway contains many genes with a large hypermethylation effect; while the p53 pathway carries more genes with a hypomethylation effect. To illustrate the differences in paired DNAm values, Fig. 5B contains a heatmap of 50 probes under the p53 pathway with the largest probabilities of hypermethylation or hypomethylation. It is well-known that the mTor pathway and the p53 pathway play an important role in cancer cell biology. A previous study of breast cancer showed that several genes downstream to *TP53* and/or estrogen receptors were regulated through DNA methylation changes⁴⁸, which agrees with our results that the methylation level of the p53 pathway was affected. Intriguingly, among the hypermethylated genes in the mTor pathway, a previous report has demonstrated that *STK11* was highly methylated in papillary breast carcinoma and its epigenetic dysregulation may be associated with Peutz-Jeghers syndrome⁴⁹.

Discussion

The advantage of our proposed approach is its ability to start with a list of candidate pathways, and to examine in a unified analysis the effect of each pathway, while controlling for CGI status and pathway structures. Such an approach is useful when researchers have already identified specific competing pathways for further investigation. This approach can quantify the degree of importance among candidate pathways and simultaneously provide methylation information for each gene symbol. Our method can serve as a complementary tool to target pathways or certain gene ontology (GO) terms for further investigation of their molecular function.

Traditional approaches usually perform single-marker tests in the first stage, and next conduct a hypergeometric test for pathway analysis using those gene symbols that have passed the test performed in the first stage. In the second stage, each pathway is tested separately, and no intra-pathway information is considered. We call this *two-stage inference*. Most current methods use online bioinformatics tools and consult databases for annotations. For the purpose of comparison, we considered two procedures. The first applied paired t-tests with Bonferroni correction and then used DAVID for pathway analysis. No pathway was found statistically significant, unless a less stringent significance level of 0.10 was used: pathway of vascular smooth muscle contraction ($p = 0.067$), pathways in cancer ($p = 0.073$), and pathway in prostate cancer ($p = 0.084$). Except for the pathways in cancer, which was identified with our proposed model, these pathways are not associated with ovarian cancer, at least not

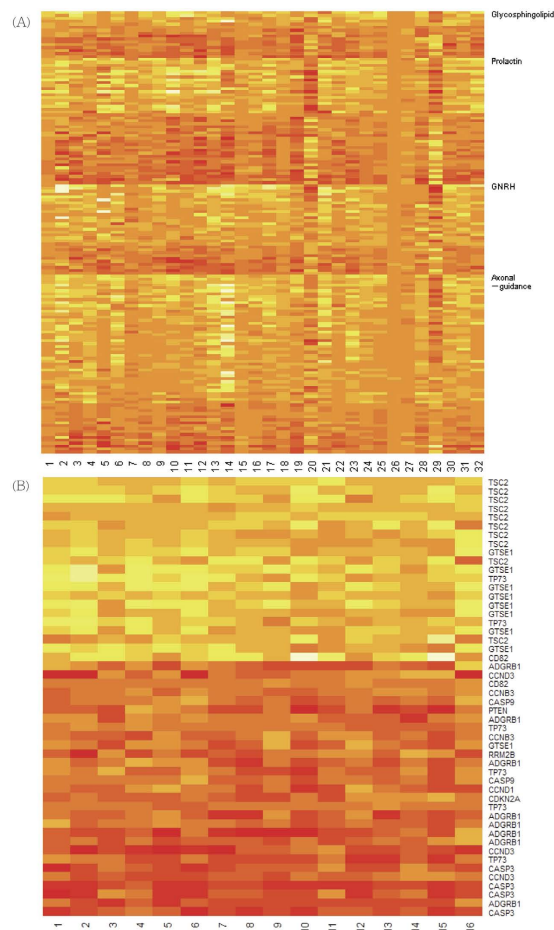


Figure 5. (A) Heatmap of differences in DNAm for leading probes. (A) These probes are those having the largest probabilities of hypermethylation (yellow) or hypomethylation (red), under each competing pathway in the lung cancer study. (B) These probes are the top 50 probes with the largest probabilities of hypermethylation (yellow) or hypomethylation (red) in the p53 pathway.

according to the current literature. In the second comparison, we considered the model with the null pathway effect (a), selected the genes with large probability of hypermethylation or hypomethylation, and then applied DAVID for pathway analyses. A total of 116 genes passed the criterion and two pathways were identified as significant, including the pathways in cancer ($p < 0.001$), and the p53 signaling pathway ($p = 0.025$) based on the modified Fisher exact tests in the DAVID annotation system. Although this procedure did not pick up the cell cycle pathway as our proposed model did, the p53 signaling pathway, which it did identify, can be activated by stress signals, resulting in three major outputs: cell cycle arrest, cellular senescence or apoptosis.

When applying the proposed analysis, other functional forms of pathway topology can be considered. For instance, correlations among genes can replace the number of connecting genes to describe the interaction. Pathways can be extended to networks so that the crosstalk between pathways can be examined, including a network of networks or even the whole interactome⁵⁰. Scientists have observed that some highly connected genes, called hubs, are usually more ancient and give rise to diversified and abundant phenotypes⁵¹. In that case, the effect of an individual gene may be inversely proportional to its number of links. Therefore, instead of using a simple count of the number of edges linking each gene to the others in a given pathway, an alternative would be to replace the functions in models (c1) and (c2) with analogous functions that model the inverse-degree effect. More details about how to do this in practice can be found in Supplementary Text S1.

Methods

Statistical models and pathway effect specifications. In our proposed model for the matched case-control study, each θ_{ij} denotes the observed difference in DNA methylation levels at the j th probe (P_j) between the i th case-control pair recruited. Each θ_{ij} follows a normal distribution with mean μ_{ij} , where μ_{ij} depends on the probe-specific parameter λ_j . This λ_j can be decomposed into two parts, one (β_j) for the effect of CGI status and the other (Φ) for the pathway effect. Those probes located in CGI share a common effect from the distribution $N(0, \sigma_{\beta_2}^2)$; while those probes not in CGI share another common effect from a different distribution $N(0, \sigma_{\beta_1}^2)$. These two distributions allow the pathway effect to depend on CGI status, and allow the variability of the pathway effect to vary when CGI status differs.

		Difference in DNAm		Difference in Gene Exp	
		Mean	SD	Mean	SD
Pr(hypermethylation)					
<i>ABLIM1</i>	>0.99	0.14	0.11	-0.82	0.54
<i>DCC</i>	>0.99	0.14	0.16	-0.36	0.28
<i>EFNA2</i>	0.96	0.07	0.13	-0.05	0.22
<i>EFNB1</i>	0.98	0.07	0.08	-0.27	0.38
<i>EPHA5</i>	0.99	0.08	0.09	-0.12	0.30
<i>EPHA8</i>	0.96	0.06	0.07	0.09	0.23
<i>LIMK1</i>	0.99	0.10	0.12	0.36	0.24
<i>LRRC4</i>	0.98	0.11	0.15	-0.29	0.40
<i>NTNG1</i>	0.96	0.06	0.07	-0.67	0.47
<i>PAK2</i>	>0.99	0.13	0.13	-0.08	0.47
<i>PAK7</i>	0.97	0.08	0.12	0.08	0.13
<i>PLXNB1</i>	0.99	0.13	0.17	<0.01	0.13
<i>SEMA3G</i>	0.99	0.09	0.08	-1.72	1.35
<i>SEMA3E</i>	0.91	0.04	0.08	-1.22	1.47
<i>SLIT2</i>	0.93	0.05	0.10	-1.62	1.11
<i>SLIT3</i>	0.93	0.06	0.13	-0.44	0.38
<i>UNC5A</i>	0.92	0.06	0.13	0.06	0.21
<i>UNC5C</i>	0.91	0.05	0.11	-0.07	0.13
Pr(hypomethylation)					
<i>MAPK1</i>	>0.99	-0.15	0.14	-0.23	0.35
<i>HRAS</i>	0.97	-0.07	0.06	-0.04	0.41
<i>EPHA1</i>	0.98	-0.07	0.08	0.24	0.21
<i>NEFATC2</i>	0.91	-0.05	0.05	-0.19	0.39
<i>NGEF</i>	0.91	-0.05	0.06	0.52	0.39
<i>NTNG2</i>	0.91	-0.06	0.12	-0.23	0.35
<i>PLXNB3</i>	0.96	-0.08	0.10	0.43	0.51
<i>PPP3R2</i>	0.98	-0.10	0.12	<0.01	0.11
<i>SEMA3B</i>	0.97	-0.10	0.15	-0.60	0.43
<i>SEMA4A</i>	0.98	-0.16	0.19	<0.01	0.61
<i>SEMA4G</i>	0.93	-0.05	0.06	0.25	0.51
<i>SEMA6B</i>	0.98	-0.10	0.11	-0.06	0.41

Table 3. Genes with large probabilities of hypermethylation or hypomethylation under the axonal guidance pathway in the lung cancer study. The corresponding average and standard deviation of difference in DNA methylation and gene expression are also listed.

For the function of the pathway effect $\Phi(\boldsymbol{\gamma}; P_j, \boldsymbol{\Lambda})$, P_j is the probe and $\boldsymbol{\Lambda}$ contains all pathways $\{\Lambda_1, \Lambda_2, \dots, \Lambda_K\}$ of interest with $\boldsymbol{\gamma} = (\gamma_1, \gamma_2, \dots, \gamma_K)$ as the corresponding parameters. To simplify the notation, we assume that the joint-effect Φ can be partitioned into $f_k(P_j)$, where $k = 1, \dots, K$. That is, $\Phi(\boldsymbol{\gamma}; P_j, \boldsymbol{\Lambda}) = \sum_{k=1}^K f_k(P_j)$.

Each $f_k(P_j)$ can be defined according to various scenarios. If each pathway has no effect on methylation, then $\Phi(\boldsymbol{\gamma}; P_j, \boldsymbol{\Lambda}) = 0$. This is the null effect model, denoted as model (a). For the case where all genes share the same pathway effect, we consider $f_k(P_j) = I_k(P_j) \times \gamma_k$, and called the CGI-independent constant pathway effect model (b1). However, inside the same pathway, if the effect differs because of CGI status, then the pathway effect would be decomposed into two terms, $f_k(P_j) = I_k(P_j) \times \gamma_k^C$ if the probe P_j is in CGI and $f_k(P_j) = I_k(P_j) \times \gamma_k^{nC}$ if not. This is called the CGI-dependent constant pathway effect model (b2).

It is possible that the role of a gene depends on its position in a given pathway¹³. For example, the number of its neighboring genes E_{jk} may imply that this gene is a hub gene and is influential in maintaining the integrity and normal function of the pathway¹⁵. In network analysis, the number of incoming and outgoing links per node (gene) in a network is called the *degree* or *connectivity*, which can influence the performance of the network. Thus we consider $f_k(P_j) = E_{jk} \times \gamma_k$, and call it the CGI-independent degree effect model (c1). When such an effect is modified by CGI status, then it is assumed $f_k(P_j) = E_{jk} \times \gamma_k^C$ if the probe P_j is in CGI and $f_k(P_j) = E_{jk} \times \gamma_k^{nC}$ if not. This is the CGI-dependent degree effect model (c2). The deviance information criterion (DIC) is a common measure in Bayesian analysis for model selection. Here we derived the DIC for each model and selected model (b2) as the final model. All probabilities and inference are based on this model.

Computations. All the statistical inference was made based on the posterior probability of the parameter of interest, where the probability is evaluated based on samples derived from the Markov chain Monte Carlo method (MCMC). In the above modeling, γ_k measures the strength of association between the k th pathway and the

P53 pathway		Difference in DNAm		Difference in Gene Exp	
Pr(hypermethylation)		Mean	SD	Mean	SD
<i>GTSE1</i>	0.91	0.20	0.11	2.65	0.83
<i>TSC2</i>	0.95	0.19	0.07	0.09	0.61
Pr(hypomethylation)					
<i>ADGRB1</i>	0.95	-0.29	0.10	-	-
<i>CASP3</i>	0.96	-0.31	0.11	-0.22	0.46
<i>CASP9</i>	0.91	-0.13	0.10	0.58	0.42
<i>CCND1</i>	0.91	-0.15	0.16	1.48	1.17
<i>CCND3</i>	0.94	-0.18	0.10	-0.06	0.51
<i>CDKN2A</i>	0.91	-0.15	0.14	1.34	0.86
<i>TP73</i>	0.93	-0.25	0.14	1.11	0.66
mTor pathway					
Pr(hypermethylation)					
<i>AKT3</i>	0.94	0.22	0.15	-1.87	0.83
<i>EIF4E2</i>	0.95	0.17	0.13	-1.10	0.56
<i>INS</i>	0.95	0.24	0.17	-	-
<i>PDPK1</i>	0.91	0.21	0.19	-0.04	0.39
<i>PIK3CB</i>	0.97	0.20	0.08	-0.60	0.63
<i>PIK3CD</i>	0.95	0.18	0.12	-0.39	1.28
<i>PIK3R3</i>	0.94	0.15	0.11	1.08	0.73
<i>PRKCA</i>	0.94	0.23	0.15	-0.50	1.21
<i>PRKCB</i>	0.95	0.18	0.07	3.45	1.77
<i>PRKCG</i>	0.95	0.18	0.12	-	-
<i>RPS6KA1</i>	0.92	0.12	0.08	-1.36	0.54
<i>RPS6KA2</i>	0.95	0.15	0.08	-1.22	0.71
<i>RPTOR</i>	0.97	0.23	0.10	0.04	0.77
<i>STK11</i>	0.96	0.20	0.11	-0.12	0.38
<i>TSC2</i>	0.95	0.19	0.07	0.09	0.61
Pr(hypomethylation)					
<i>PDPK1</i>	0.92	-0.20	0.06	-0.04	0.39

Table 4. Genes with large probabilities of hypermethylation or hypomethylation in the two pathways in the HG-DCIS study.

disease phenotype. A large value of its posterior probability $P(\gamma_k > 0 | \theta = (\theta_{ij}))$ suggests that genes in the k th pathway tend to be more hypermethylated in cancer patients (cases) than in healthy subjects (controls); while a small value implies more hypomethylation in cases than in controls. Similarly, large values of the posterior probabilities $\gamma_k^C > 0$ (or $\gamma_k^{nC} > 0$) indicate that genes with probes in CGI regions (or non-CGI regions) are more likely to be hypermethylated among the cancer subjects.

To evaluate the degree of association between the gene G_j and the phenotype, we examined the association between the j th probe and the disease by evaluating the conditional probability $P(\lambda_j > 0 | \theta = (\theta_{ij}))$. A probability close to one suggests greater hypermethylation among the cases; a value closer to zero suggests hypomethylation.

References

- Heyn, H. & Esteller, M. DNA methylation profiling in the clinic: applications and challenges. *Nat Rev Genet* **13**, 679–692 (2012).
- Chiam, K., Ricciardelli, C. & Bianco-Miotto, T. Epigenetic biomarkers in prostate cancer: Current and future uses. *Cancer Lett* **342**, 248–256 (2014).
- Rakyan, V. K., Down, T. A., Balding, D. J. & Beck, S. Epigenome-wide association studies for common human diseases. *Nat Rev Genet* **12**, 529–541 (2011).
- Chao, C., Chi, M., Preciado, M. & Black, M. H. Methylation markers for prostate cancer prognosis: a systematic review. *Cancer Causes Control* **24**, 1615–1641 (2013).
- Feinberg, A. P. & Irizarry, R. A. Evolution in health and medicine Sackler colloquium: Stochastic epigenetic variation as a driving force of development, evolutionary adaptation, and disease. *Proc Natl Acad Sci USA* **107** Suppl 1, 1757–1764 (2010).
- Rodriguez-Paredes, M. & Esteller, M. Cancer epigenetics reaches mainstream oncology. *Nat Med* **17**, 330–339 (2011).
- Deaton, A. M. & Bird, A. CpG islands and the regulation of transcription. *Genes Dev* **25**, 1010–1022 (2011).
- Illingworth, R. S. & Bird, A. P. CpG islands—a rough guide. *FEBS Lett* **583**, 1713–1720 (2009).
- Gardiner-Garden, M. & Frommer, M. CpG islands in vertebrate genomes. *J Mol Biol* **196**, 261–282 (1987).
- Das, P. M. & Singal, R. DNA methylation and cancer. *J Clin Oncol* **22**, 4632–4642 (2004).
- Esteller, M. Cancer epigenomics: DNA methylomes and histone-modification maps. *Nat Rev Genet* **8**, 286–298 (2007).
- McCabe, M. T., Brandes, J. C. & Vertino, P. M. Cancer DNA methylation: molecular mechanisms and clinical implications. *Clin Cancer Res* **15**, 3927–3937 (2009).
- Draghici, S. *et al.* A systems biology approach for pathway level analysis. *Genome Res* **17**, 1537–1545 (2007).
- Tarca, A. L. *et al.* A novel signaling pathway impact analysis. *Bioinformatics* **25**, 75–82 (2009).

15. Luscombe, N. M. *et al.* Genomic analysis of regulatory network dynamics reveals large topological changes. *Nature* **431**, 308–312 (2004).
16. Christensen, B. C. *et al.* Aging and environmental exposures alter tissue-specific DNA methylation dependent upon CpG island context. *PLoS Genet* **5**, e1000602 (2009).
17. Gaidatzis, D. *et al.* DNA sequence explains seemingly disordered methylation levels in partially methylated domains of Mammalian genomes. *PLoS Genet* **10**, e1004143 (2014).
18. Zhang, B. *et al.* Functional DNA methylation differences between tissues, cell types, and across individuals discovered using the M&M algorithm. *Genome Res* **23**, 1522–1540 (2013).
19. Ma, B. *et al.* Predicting DNA methylation level across human tissues. *Nucleic Acids Res* **42**, 3515–3528 (2014).
20. Teschendorff, A. E. *et al.* Age-dependent DNA methylation of genes that are suppressed in stem cells is a hallmark of cancer. *Genome Res* **20**, 440–446 (2010).
21. Florath, I., Butterbach, K., Muller, H., Bewerunge-Hudler, M. & Brenner, H. Cross-sectional and longitudinal changes in DNA methylation with age: an epigenome-wide analysis revealing over 60 novel age-associated CpG sites. *Hum Mol Genet* **23**, 1186–1201 (2014).
22. Horvath, S. *et al.* Aging effects on DNA methylation modules in human brain and blood tissue. *Genome Biol* **13**, R97 (2012).
23. Martino, D. *et al.* Longitudinal, genome-scale analysis of DNA methylation in twins from birth to 18 months of age reveals rapid epigenetic change in early life and pair-specific effects of discordance. *Genome Biol* **14**, R42 (2013).
24. Jaffe, A. E. *et al.* Bump hunting to identify differentially methylated regions in epigenetic epidemiology studies. *Int J Epidemiol* **41**, 200–209 (2012).
25. Down, T. A. *et al.* A Bayesian deconvolution strategy for immunoprecipitation-based DNA methylome analysis. *Nat Biotechnol* **26**, 779–785 (2008).
26. Jeong, J. *et al.* An empirical Bayes model for gene expression and methylation profiles in antiestrogen resistant breast cancer. *BMC Med Genomics* **3**, 55 (2010).
27. Lu, T. P. *et al.* Identification of regulatory SNPs associated with genetic modifications in lung adenocarcinoma. *BMC Res Notes* **8**, 92 (2015).
28. Abba, M. C. *et al.* A Molecular Portrait of High-Grade Ductal Carcinoma *In Situ*. *Cancer Res* **75**, 3980–3990 (2015).
29. Fu, L. J. & Wang, B. Investigation of the hub genes and related mechanism in ovarian cancer via bioinformatics analysis. *J Ovarian Res* **6**, 92 (2013).
30. Kanehisa, M. *et al.* Data, information, knowledge and principle: back to metabolism in KEGG. *Nucleic Acids Res* **42**, D199–D205 (2014).
31. Kanehisa, M. & Goto, S. KEGG: kyoto encyclopedia of genes and genomes. *Nucleic Acids Res* **28**, 27–30 (2000).
32. Ruklisa, D., Ware, J. S., Walsh, R., Balding, D. J. & Cook, S. A. Bayesian models for syndrome- and gene-specific probabilities of novel variant pathogenicity. *Genome Med* **7**, 5 (2015).
33. Das, A. *et al.* Bayesian integration of genetics and epigenetics detects causal regulatory SNPs underlying expression variability. *Nat Commun* **6**, 8555 (2015).
34. Villarreal, J. C. & Renner, S. S. Hornwort pyrenoids, carbon-concentrating structures, evolved and were lost at least five times during the last 100 million years. *Proc Natl Acad Sci USA* **109**, 18873–18878 (2012).
35. Scheitz, C. J., Lee, T. S., McDermitt, D. J. & Tumber, T. Defining a tissue stem cell-driven Runx1/Stat3 signalling axis in epithelial cancer. *EMBO J* **31**, 4124–4139 (2012).
36. Sheng, Q. & Liu, J. The therapeutic potential of targeting the EGFR family in epithelial ovarian cancer. *Br J Cancer* **104**, 1241–1245 (2011).
37. Silver, D. L., Naora, H., Liu, J., Cheng, W. & Montell, D. J. Activated signal transducer and activator of transcription (STAT) 3: localization in focal adhesions and function in ovarian cancer cell motility. *Cancer Res* **64**, 3550–3558 (2004).
38. Zhao, R. *et al.* DDB2 modulates TGF-beta signal transduction in human ovarian cancer cells by downregulating NEDD4L. *Nucleic Acids Res* **43**, 7838–7849 (2015).
39. Potiron, V. A., Roche, J. & Drabkin, H. A. Semaphorins and their receptors in lung cancer. *Cancer Lett* **273**, 1–14 (2009).
40. Lu, T. P. *et al.* Identification of a novel biomarker, SEMA5A, for non-small cell lung carcinoma in nonsmoking women. *Cancer Epidemiol Biomarkers Prev* **19**, 2590–2597 (2010).
41. Nasarre, P., Potiron, V., Drabkin, H. & Roche, J. Guidance molecules in lung cancer. *Cell Adh Migr* **4**, 130–145 (2010).
42. Guo, B. *et al.* (-)-beta-hydrastine suppresses the proliferation and invasion of human lung adenocarcinoma cells by inhibiting PAK4 kinase activity. *Oncol Rep* **35**, 2246–2256 (2016).
43. Lee, M. O. *et al.* p16Ink4a suppression of lung adenocarcinoma by Bmi-1 in the presence of p38 activation. *J Thorac Oncol* **6**, 423–431 (2011).
44. Soans, E., Evans, S. C., Cipolla, C. & Fernandes, E. Characterizing the sphingomyelinase pathway triggered by PRIMA-1 derivatives in lung cancer cells with differing p53 status. *Anticancer Res* **34**, 3271–3283 (2014).
45. Le Bescont, A. *et al.* Receptor-Independent Ectopic Activity of Prolactin Predicts Aggressive Lung Tumors and Indicates HDACi-Based Therapeutic Strategies. *Antioxid Redox Signal* **23**, 1–14 (2015).
46. Lu, C., Huang, T., Chen, W. & Lu, H. GnRH participates in the self-renewal of A549-derived lung cancer stem-like cells through upregulation of the JNK signaling pathway. *Oncol Rep* **34**, 244–250 (2015).
47. Marien, E. *et al.* Non-small cell lung cancer is characterized by dramatic changes in phospholipid profiles. *Int J Cancer* **137**, 1539–1548 (2015).
48. Ung, M. H., Varn, F. S., Lou, S. & Cheng, C. Regulators associated with clinical outcomes revealed by DNA methylation data in breast cancer. *PLoS Comput Biol* **11**, e1004269 (2015).
49. Esteller, M. *et al.* Epigenetic inactivation of LKB1 in primary tumors associated with the Peutz-Jeghers syndrome. *Oncogene* **19**, 164–168 (2000).
50. Barabasi, A. L. & Oltvai, Z. N. Network biology: understanding the cell's functional organization. *Nat Rev Genet* **5**, 101–113 (2004).
51. Vidal, M., Cusick, M. E. & Barabasi, A. L. Interactome networks and human disease. *Cell* **144**, 986–998 (2011).

Acknowledgements

This work was supported by Ministry of Science and Technology, 103-2314-B-002-039-MY3.

Author Contributions

C.-W.C., C.-X.S. and Y.-C.F. carried out the data analysis and statistical inference. C.-W.C., T.-P.L. and C.K.H. conceived the analysis and helped write the manuscript.

Additional Information

Supplementary information accompanies this paper at <http://www.nature.com/srep>

Competing financial interests: The authors declare no competing financial interests.

How to cite this article: Chang, C.-W. *et al.* Gene-set Analysis with CGI Information for Differential DNA Methylation Profiling. *Sci. Rep.* **6**, 24666; doi: 10.1038/srep24666 (2016).



This work is licensed under a Creative Commons Attribution 4.0 International License. The images or other third party material in this article are included in the article's Creative Commons license, unless indicated otherwise in the credit line; if the material is not included under the Creative Commons license, users will need to obtain permission from the license holder to reproduce the material. To view a copy of this license, visit <http://creativecommons.org/licenses/by/4.0/>